Journal of Alloys and Compounds 488 (2009) 339–345

Contents lists available at ScienceDirect

Journal of Alloys and Compounds

journal homepage: www.elsevier.com/locate/jallcom

Magnetic greigite (Fe_3S_4) nanomaterials: Shape-controlled solvothermal synthesis and their calcination conversion into hematite (α-Fe_2O_3) nanomaterials

Zhong Jie Zhang[a,*], Xiang Ying Chen[b]

[a] College of Chemistry and Chemical Engineering, Key Laboratory of Environment-friendly Polymer Materials of Anhui Province, Anhui University, Hefei, Anhui 230039, PR China
[b] School of Chemical Engineering, Anhui Key Laboratory of Controllable Chemistry Reaction & Material Chemical Engineering, Hefei University of Technology, Hefei, Anhui 230009, PR China

ARTICLE INFO

Article history:
Received 4 August 2009
Received in revised form 24 August 2009
Accepted 25 August 2009
Available online 31 August 2009

Keywords:
Nanostructured materials
Chemical synthesis
Crystal structure
Magnetic measurements

ABSTRACT

We demonstrated here the solvothermal synthetic method to selectively prepare magnetic greigite (Fe_3S_4) nanosheets and nanoparticles in the mixed solvents of ethylene glycol (EG) and H_2O. The as-prepared Fe_3S_4 nanomaterials were further converted into hematite (α-Fe_2O_3) having branched structures under calcining conditions. The samples were well characterized by means of XRPD, FESEM, TEM, HRTEM, TGA and magnetic hysteresis curves. The experimental results reveal that the reaction parameters including the composition of mixed solvents, solvothermal temperature, and calcination temperature play important roles on achieving pure phase Fe_3S_4 and α-Fe_2O_3 samples. Significantly, we for the first time studied the elevated-temperature oxidation behavior of Fe_3S_4 sample into α-Fe_2O_3 in air, accompanying with the size and shape changing dramatically. The magnetic hysteresis curves of Fe_3S_4 show the ferromagnetic behaviors at room temperature.

1. Introduction

In the past decades, shape control of nanostructures as we desire has been proved extremely important because a wide range of physical and chemical properties depend primarily on their sizes and shapes [1–3]. For example, optical or catalytic properties of rare-earth oxide nanocrystals [4], CdTe tetrapods [5], Cu_2O coated with Cu nanoparticles [6], and Rh nanoparticles on charcoal [7] are strongly dependent on their shapes.

Fe_3S_4, designated as greigite, was first proposed as a mineral by Skinner et al. [8]. Its crystal structure can be described as a *ccp* array of S atoms with Fe^{3+} occupying one-eighth of the available tetrahedral voids and Fe^{2+} and Fe^{3+} randomly distributed over one-half of the available octahedral voids [9]. Greigite was identified in many natural environments of up to a few million years old [10], and it could act as an indicator of drought [11]. Meanwhile, the natural Fe_3S_4 sample presents a core-shell structure of crystallized greigite surrounded by an amorphous iron oxide phase [12]. Besides, electron hopping is inferred to occur between high-spin ferric and ferrous iron in octahedral lattice positions in greigite, a property could thus result in metallic conductivity [13]. Spender et al. [14] determined the conductivity of greigite to be semi-metallic owing to non-stoichiometry to Fe-vacancies on the octahedral lattice sites.

So far, there have been only a small quantity of nanoscale greigite reported in the literature mainly because it has a limited stability against pH and dissolved sulfur activity [10]. Fe_3S_4 and FeS_2 nanoparticles were selectively prepared via the toluene-thermal method [15]; Yu and co-workers reported the *in situ* magnetic-field-assisted hydrothermal route to prepare microrods of Fe_3S_4 and FeS_2 [16]; O'Brien and Vanitha prepared magnetic iron sulfide nanocrystals including Fe_3S_4 and Fe_7S_8 from a cubane-type Fe-S cluster [17]. Furthermore, we have developed a simple hydrothermal method to controllably prepare Fe_3S_4 samples using $FeCl_3{\cdot}6H_2O$ or $FeSO_4{\cdot}7H_2O$ and thioacetamide as raw materials, in which the reaction temperature plays the crucial role for preparing pure Fe_3S_4 [18]. On the other hand, we once prepared magnetite (Fe_3O_4) hollow spheres in absolute ethylene glycol (EG) using $FeCl_3{\cdot}6H_2O$ and $CO(NH_2)_2$ as the raw materials, in which EG can act as favorable solvent and reducing agent [19]. Given the fact that cubic Fe_3S_4 is a typical analogue of magnetite, we thus proposed to prepare it by virtue of EG in this study.

Herein, a solvothermal synthetic method has been developed to prepare greigite (Fe_3S_4) samples in the mixed solvents of ethylene glycol (EG) and H_2O. And then, the as-prepared Fe_3S_4 nanomaterials were converted into hematite (α-Fe_2O_3) by calcination method. In particular, as far as we know, it is the first report on the elevated-

* Corresponding author. Tel.: +86 551 2901450; fax: +86 551 2901450.
E-mail address: cxyhfut@gmail.com (Z.J. Zhang).

0925-8388/$ – see front matter © 2009 Elsevier B.V. All rights reserved.
doi:10.1016/j.jallcom.2009.08.127

temperature oxidation behavior of Fe_3S_4 sample into α-Fe_2O_3 in air. The magnetic properties of Fe_3S_4 samples having various shapes were measured at room temperature.

2. Experimental

All the chemicals are of analytical grade and used as received without further purification. The experiments were carried out in a 50 mL Teflon-lined stainless steel autoclave by adjusting the volume compositions of mixed solvents (EG + H_2O) (i.e., pure 40 mL EG; 30 mL + 10 mL; 20 mL + 20 mL; 10 mL + 30 mL; and pure 40 mL H_2O), the reaction temperature (i.e., 120 °C; 140 °C; 160 °C; 180 °C; and 200 °C) and the calcination temperature (i.e., 300 °C; 400 °C; 500 °C; 600 °C; 700 °C and 800 °C) in air.

2.1. Solvothermal preparation of Fe_3S_4 nanoparticles in mixed solvents (EG + H_2O)

$FeCl_3·6H_2O$ (2 mmol) and thiourea (4 mmol) were dissolved in mixed solvents (EG + H_2O = 30 mL + 10 mL) to form carmine solution under magnetic stirring. After that, the above solution was transferred into a 50 mL Teflon-lined stainless steel autoclave, which was further sealed and kept at 180 °C in an electrical oven. After 12 h, the resulting black powder was filtered off, washed with distilled water and absolute ethanol for several times, and then dried under vacuum at 60 °C for 6 h.

2.2. Post-calcining preparation of α-Fe_2O_3 sample in air

The as-prepared Fe_3S_4 sample was post-calcined at 600 °C for 3 h in a horizontal furnace in air, finally resulting in the brick red α-Fe_2O_3 sample.

2.3. Characterization

X-ray powder diffraction (XRPD) patterns were obtained on a Rigaku Max-2200 X-ray diffractometer equipped with graphite monochromatized Cu K_α radiation. Transmission electron microscope (TEM) and high-resolution TEM (HRTEM) images were taken with a JEOL 2100F unit operated at 200 kV. Field emission scanning electron microscopy (FESEM) images were taken with a Hitachi S-4800 scanning electron microscope. The thermogravimetric analysis (TGA) was conducted using a Shimadzu TGA-50H analyzer. The magnetic measurement was carried out in a vibrating sample magnetometer (VSM) (BHV-55, Riken, Japan).

3. Results and discussion

The phase, crystallinity and purity of samples prepared under various conditions were determined by means of XRPD technique. As is known, the shape, size and phase formation for various nanocrystals under solvothermal conditions strongly depend on solvent effects (i.e., polarity, viscosity, and softness), which will influence the solubility and transport behavior of the precursors [20]. In the present case, we principally studied the impact of volume compositions of mixed solvents (EG + H_2O) on crystal growth and phase formation. When conducting the reaction system containing $FeCl_3·6H_2O$ and thiourea as raw materials at 180 °C for 12 h in pure 40 mL EG, the resulting black powder occurred. Its corresponding XRPD pattern is shown in Fig. 1a, whose reflection peaks can be readily indexed as cubic Fe_3S_4 (JCPDS file No. 89-1998). Next, when adjusting the volume composition (EG + H_2O) as 30 mL + 10 mL and keeping other reaction parameters unchanged, the resultant sample can also be indentified as cubic Fe_3S_4 (JCPDS file No. 89-1998), as shown in Fig. 1b. However, compared with the XRPD patterns in Fig. 1a and b, we can see that a little discrepancy exists between their reflection peaks including the position, intensity and broadness. This kind of result indicates that the characteristics of these two samples will differ. When further altering the volume composition (EG + H_2O) as 30 mL + 10 mL or 20 mL + 20 mL and keeping other reaction parameters unchanged, the resulting samples in Fig. 1c and d are both mixtures composed of cubic Fe_3S_4 (JCPDS file No. 89-1998), orthorhombic FeS_2 (JCPDS file No. 37-0475), and cubic FeS_2 (JCPDS file No. 42-1340). Besides, when conducting the reaction system containing $FeCl_3·6H_2O$ and thiourea as raw materials at 180 °C for 12 h in pure 40 mL H_2O, the

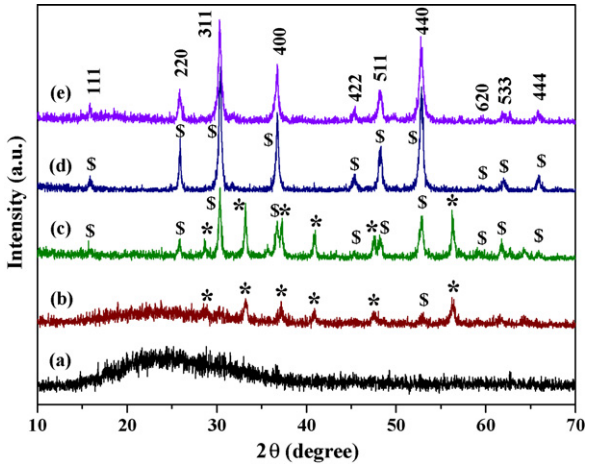

Fig. 2. XRPD patterns of the samples prepared for 12 h in fixed volume compositions (EG + H_2O = 30 mL + 10 mL) at various reaction temperatures, using $FeCl_3·6H_2O$ and thiourea as raw materials; (a) 120 °C; (b) 140 °C; (c) 160 °C; (d) 180 °C; (e) 200 °C. Notes: $ = cubic Fe_3S_4 (JCPDS file No. 89-1998), and * = cubic FeS_2 (JCPDS file No. 42-1340).

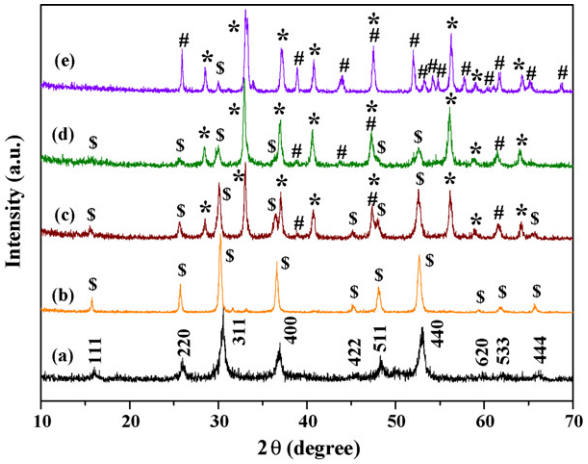

Fig. 1. XRPD patterns of the samples prepared at 180 °C for 12 h with various volume compositions (EG + H_2O), using $FeCl_3·6H_2O$ and thiourea as raw materials: (a) pure 40 mL EG; (b) 30 mL + 10 mL; (c) 20 mL + 20 mL; (d) 10 mL + 30 mL; (e) pure 40 mL H_2O. Notes: $ = cubic Fe_3S_4 (JCPDS file No. 89-1998), # = orthorhombic FeS_2 (JCPDS file No. 37-0475), and * = cubic FeS_2 (JCPDS file No. 42-1340).

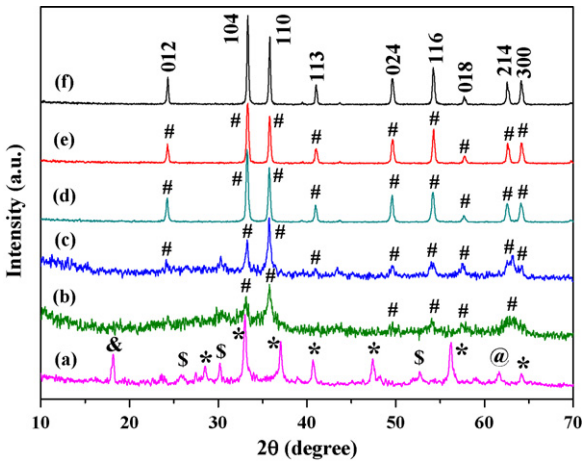

Fig. 3. XRPD patterns of the samples obtained by calcining Fe_3S_4 sample at various reaction temperatures; (a) 300 °C; (b) 400 °C; (c) 500 °C; (d) 600 °C; (e) 700 °C; (f) 800 °C. Notes: # = hexagonal α-Fe_2O_3 (JCPDS file No. 33-0664), $ = cubic Fe_3S_4 (JCPDS file No. 89-1998), @ = orthorhombic FeS_2 (JCPDS file No. 37-0475), & = hexagonal FeS (JCPDS file No. 37-0477), and * = cubic FeS_2 (JCPDS file No. 42-1340).

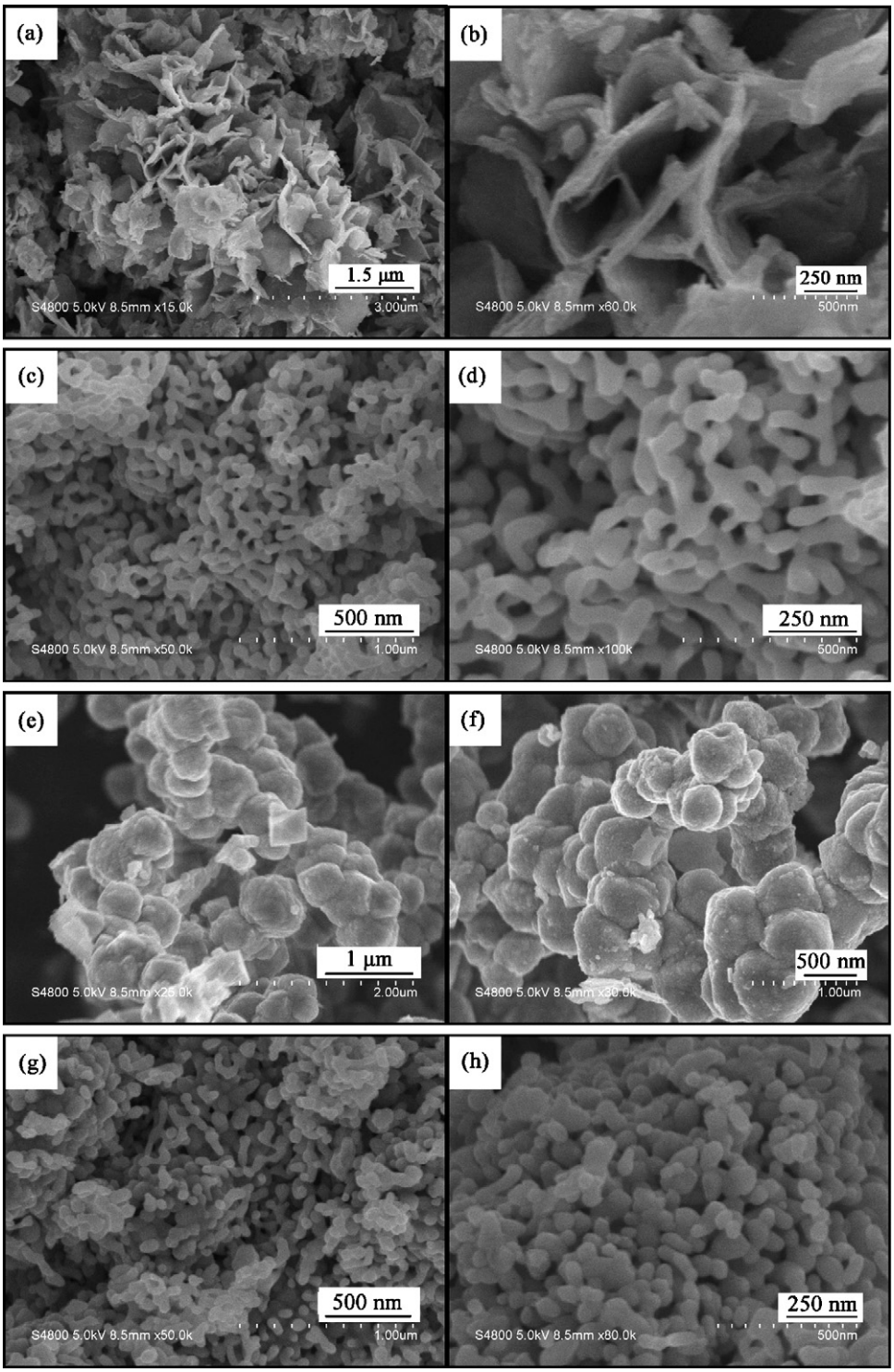

Fig. 4. (a and b) FESEM images of Fe_3S_4 sample obtained in pure 40 mL EG and their conversion into (c and d) α-Fe_2O_3 calcined at 700 °C for 3 h; (e and f) FESEM images of Fe_3S_4 sample obtained in mixed solvents of EG and H_2O (30 mL + 10 mL) and their conversion into (g and h) α-Fe_2O_3 calcined at 700 °C for 3 h.

corresponding sample mainly consists of orthorhombic FeS_2 (JCPDS file No. 37-0475), and cubic FeS_2 (JCPDS file No. 42-1340), as shown in Fig. 1e.

On the other hand, in order to investigate the influence of reaction temperature on the formation of cubic Fe_3S_4, we carried out a series of experiments at various reaction temperatures for 12 h using $FeCl_3{\cdot}6H_2O$ and thiourea as raw materials while fixing the volume composition (EG + H_2O) as 30 mL + 10 mL. Fig. 2a is the typical XRPD pattern of the sample obtained at 120 °C while keeping other reaction parameters constant, and the result tells us that the sample is amorphous. This means that low reaction temperature is not favorable for producing crystallinic Fe_3S_4. Thus, we decided to enhance the reaction temperature from 120 °C to 140 °C, and the resulting XRPD pattern is given in Fig. 2b. It is obvious to us that the as-prepared sample is still of bad crystallinity, although some weak reflection peaks attributable to cubic FeS_2 (JCPDS file No. 42-1340) appear. When increasing the reaction temperature to 160 °C, the resultant sample in Fig. 2c is well crystallized and

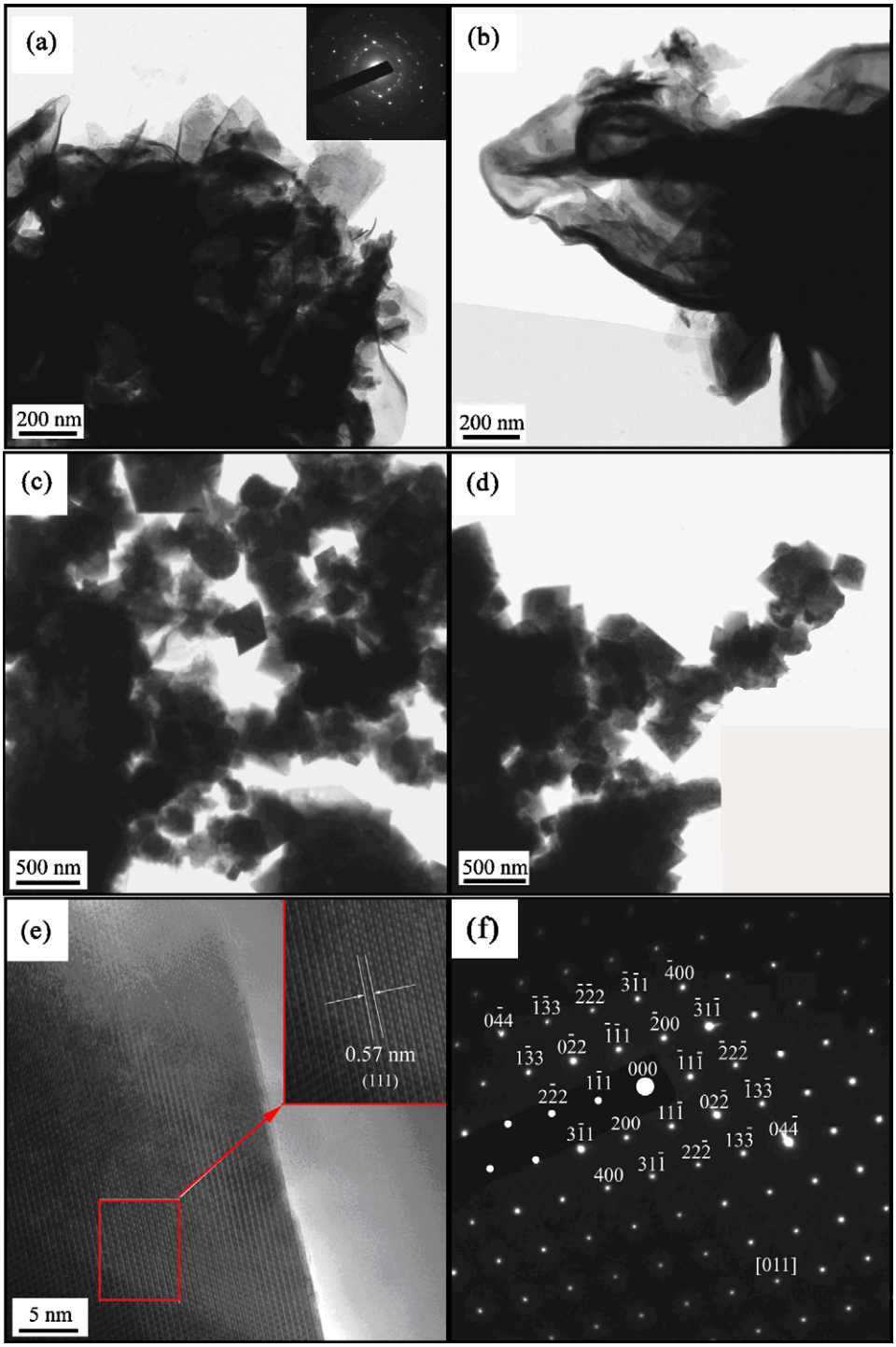

Fig. 5. TEM and HRTEM images of the Fe_3S_4 samples obtained at 180 °C for 12 h with various volume compositions (EG + H_2O): (a and b) pure 40 mL EG; (c–f) 30 mL + 10 mL.

is actually made up of cubic Fe_3S_4 (JCPDS file No. 89-1998), and cubic FeS_2 (JCPDS file No. 42-1340). To our surprise, when further increasing the reaction temperature to 180 °C, the reflection peaks assigned to cubic FeS_2 completely vanish, resulting in pure phase of cubic Fe_3S_4, as shown in Fig. 2d. As for the sample obtained at 200 °C while keeping other reaction parameters constant, its XRPD pattern in Fig. 2e is almost similar to that in Fig. 2d. In virtue of the results shown in Figs. 1 and 2, we can conclude that the composition of mixed solvents and reaction temperature for solvothermal treatment are of importance for preparing pure phase Fe_3S_4.

As is known, α-Fe_2O_3 is of much significance because its wide application as gas sensor, catalyst, pigment, lithium-ion battery and photoanode [21–23]. Hitherto, α-Fe_2O_3 nanomaterials possessing distinct characteristics were prepared via different synthetic routes. Among these routes, solution-phase route and vapor-solid route are the most common. In case of solution-phase route, ferric ions and certain kind of basic source are usually involved in solution [21]. Regarding vapor-solid route, iron oxide nanobelt and nanowires arrays can be harvested by thermal oxidation of iron substrates [22,23]. On the other hand, as we know, oxides can also be derived from its form of sulfides simply by calcination method,

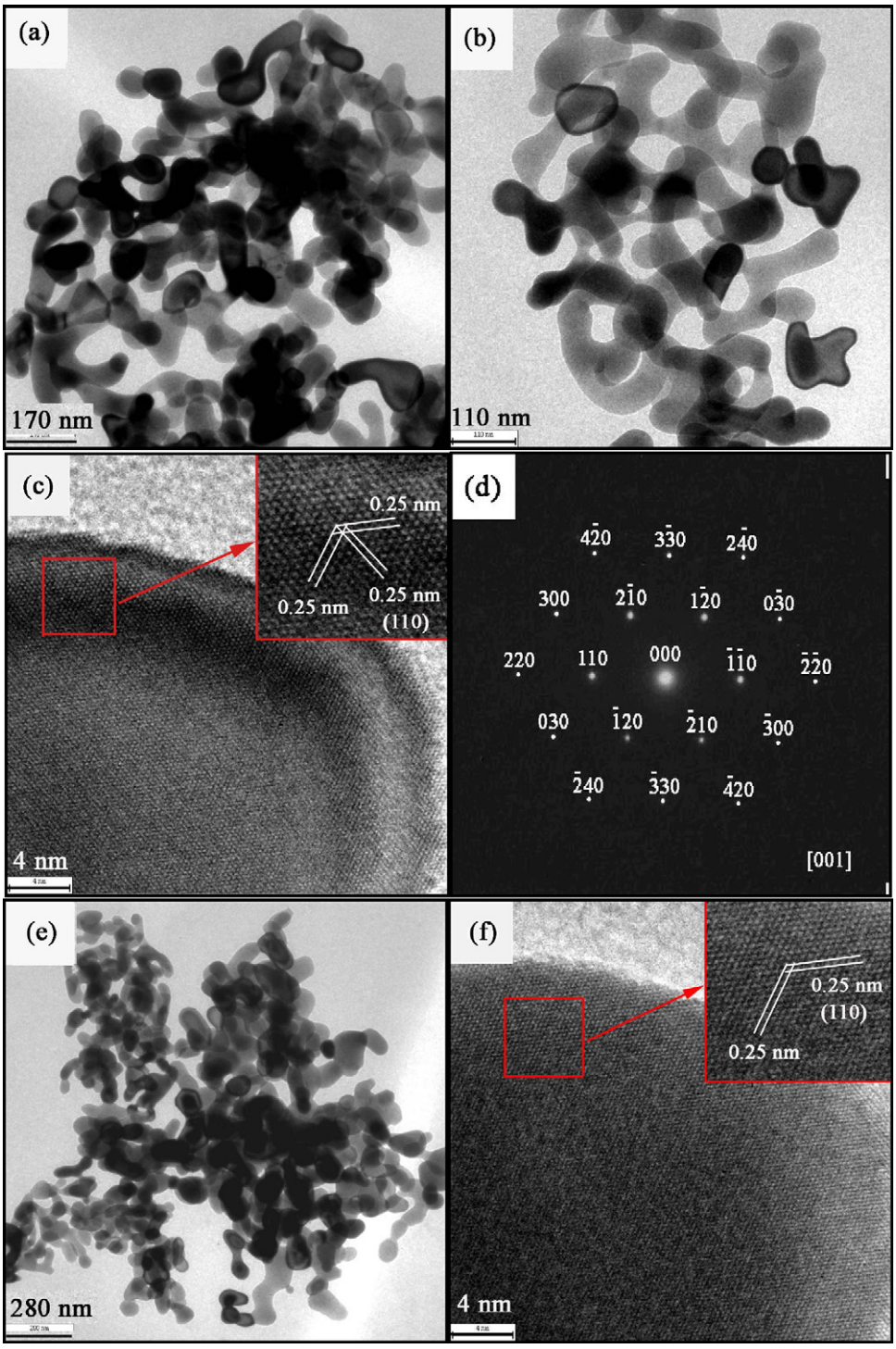

Fig. 6. TEM and HRTEM images of α-Fe_2O_3 samples obtained by the calcination of Fe_3S_4 samples, which were prepared at 180 °C for 12 h with various volume compositions (EG + H_2O): (a–d) pure 40 mL EG; (e and f) 30 mL + 10 mL.

which provides us an alternative strategy for preparing oxides. Taking In_2O_3 nanoparticles as an example, it were obtained by calcining In_2S_3 microspheres at 500 °C under ambient pressure [24]. Very recently, we prepared a series of Sb_2S_3 and Bi_2S_3 nanocrystals, which were further converted into α-Sb_2O_4 and Bi_2O_3 samples by calcination method occurring at 600 °C in air [25]. In present study, we thus planned to prepare α-Fe_2O_3 nanostructures by calcining the as-obtained cubic phase Fe_3S_4 sample at elevated-temperatures in air. Considering the fact that cubic phase Fe_3S_4 can exist steadily at 200 °C for 12 h in solution, as revealed in Fig. 2e, we chose the calcination temperature ranging from 300 °C to 800 °C to explore the elevated-temperature oxidation behavior of Fe_3S_4 sample under ambient pressure.

Fig. 3 shows us the typical XRPD patterns of the samples obtained by calcining Fe_3S_4 sample at various reaction temperatures. When designating the calcination temperature as 300 °C, the resulting product is actually mixture consisting of cubic Fe_3S_4 (JCPDS file No. 89-1998), orthorhombic FeS_2 (JCPDS file No. 37-0475), hexagonal FeS (JCPDS file No. 37-0477), and cubic FeS_2 (JCPDS file No. 42-1340), as shown in Fig. 3a. When further enhanc-

ing the calcination temperature to be 400 °C, some small reflection peaks attributable to hexagonal α-Fe_2O_3 (JCPDS file No. 33-0664) appear in Fig. 3b. To increase the crystallinity of the as-obtained sample, we manipulated the calcination temperature as high as 500 °C, 600 °C, 700 °C, and 800 °C, whose XRPD patterns are displayed in Fig. 3c–f. From these results, we find out that the higher calcination temperature, the better crystallinity of hexagonal phase α-Fe_2O_3 in nature. As a result, α-Fe_2O_3 sample were successfully obtained by calicining the as-prepared Fe_3S_4 sample in air. To the best of our knowledge, it is the first report in the literature on preparing α-Fe_2O_3 sample by the calcination of Fe_3S_4 under ambient circumstance.

FESEM technique was employed to vividly depict the genuine size and shape of the as-obtained samples. Fig. 4a and b demonstrate the representative FESEM images of Fe_3S_4 sample obtained in pure 40 mL EG. We can clearly see that the Fe_3S_4 sample consists of abundant nanosheets in nature. And then, the as-obtained Fe_3S_4 nanosheets were calcined at 700 °C for 3 h in air, giving rise to the formation of α-Fe_2O_3. Surprisingly, the resultant α-Fe_2O_3 sample takes on novel branched nanostructures, as shown in Fig. 4c and d. On the other hand, as for the Fe_3S_4 sample obtained in mixed solvents of EG and H_2O (30 mL + 10 mL), its corresponding FESEM images are displayed in Fig. 4e and f. We can see that it is composed of lots of irregular particles with *ca.* 500 nm in diameter. Afterwards, by calcining the Fe_3S_4 nanoparticles at 700 °C for 3 h in air, we obtained α-Fe_2O_3 sample, as shown in Fig. 4g and h. In like manner, the resulting α-Fe_2O_3 sample also presents branched nanostructures analogous to those in Fig. 4 c and d.

In terms of FESEM images given in Fig. 4, several scientific aspects concerning the shape and size of the as-obtained Fe_3S_4 and α-Fe_2O_3 samples deserve to be discussed. In consideration of the inverse spinel structure of greigite (Fe_3S_4), its perfect crystal structure is octahedron. However, in present study, sheet-like or grannular Fe_3S_4 sample occurred by simply altering the composition of mixed solvents containing EG and H_2O. This is caused by the solvent effect elucidated as follows: in the case of mixed solvents of EG and H_2O (30 mL + 10 mL), the addition of H_2O into EG changes the chemical properties of the solvent, such as dielectric constant, interionic attraction, and the solute–solvent interaction, which would have significant effect on the crystal growth and phase formation. In addition, the shape and size of the as-calcined branch-like α-Fe_2O_3 samples are totally different from those of their precursors of Fe_3S_4 samples. As is known, certain amount of sulfur oxides come into being in the process of oxidation behavior of Fe_3S_4 samples in air, resulting in the collapse of Fe_3S_4 crystal structure, and α-Fe_2O_3 samples having smaller sizes occur. This kind of synthetic route, which generally involves starting with a bulk solid and obtaining a nanostructure by structural decomposition, is named after "Top–down process". Taking CdO [26] and Co_3O_4 [27] nanoporous architectures as examples, they could be prepared simply by thermal decomposition of $CdCO_3$ and $CoCO_3$ in air, respectively.

Transmission electron microscopy (TEM), selected area electron diffraction (SAED), and high-resolution transmission electron microscopy (HRTEM) were performed to further investigate the crystal structure and characteristics of the as-obtained Fe_3S_4 and α-Fe_2O_3 samples. Fig. 5a and b show us the typical TEM images of the Fe_3S_4 sample obtained at 180 °C for 12 h in pure 40 mL EG. The sample consists of a great deal of nanosheets in appearance, which is in good accordance with those FESEM images shown in Fig. 4a and b. Moreover, the SAED pattern revealed as the inset in Fig. 5a tells us that this kind of Fe_3S_4 nanosheets has good crystallinity. Besides, Fig. 5c and d display the representative TEM images of the Fe_3S_4 sample obtained at 180 °C for 12 h in mixed solvents (EG + H_2O) as 30 mL + 10 mL, which are mainly composed of irregular particles. To further insight into the crystal structure of Fe_3S_4 sample, HRTEM

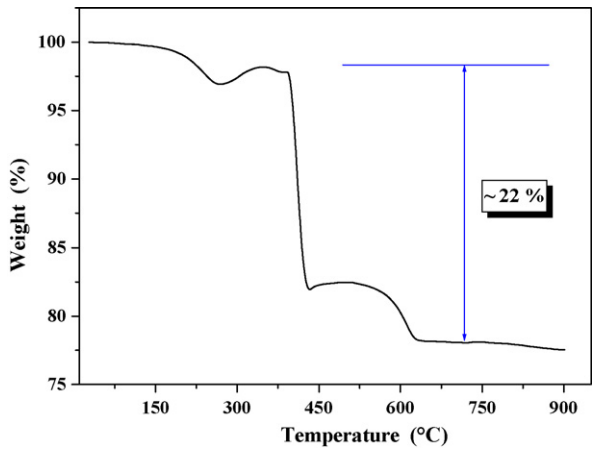

Fig. 7. TGA curve of the Fe_3S_4 sample obtained at 180 °C for 12 h in mixed solvents (EG + H_2O) as 30 mL + 10 mL.

observation was conducted, as shown in Fig. 5e. In terms of the enlarged section in Fig. 5e, we can ascertain that the lattice spacing is *ca.* 0.57 nm between two adjacent lattice planes, corresponding to that of (1 1 1) crystal planes of Fe_3S_4 sample. Besides, a typical SAED pattern randomly taken from Fe_3S_4 particles is displayed in Fig. 5f, whose zone axis is along [0 1 1] direction.

By the calcination of Fe_3S_4 nanosheets prepared at 180 °C for 12 h in pure 40 mL EG, we obtained α-Fe_2O_3 sample having novel branched structures, as shown in Fig. 6a and b. As the above-mentioned, α-Fe_2O_3 sample with various anisotropic shapes such as nanorods, nanowires, nanotubes, and nanobelts have been prepared so far [21–23]. However, the present kind of branched structures towards α-Fe_2O_3 sample is not yet reported in the literature, which might have future application in many areas. Additionally, the enlarged HRTEM image shown in Fig. 6c gives us the intrinsic structure of α-Fe_2O_3 sample, whose lattice spacing is *ca.* 0.25 nm between two adjacent lattice planes, consistent with that of (1 1 0) crystal planes of α-Fe_2O_3 sample. Fig. 6d shows the typical SAED pattern of α-Fe_2O_3 sample, whose regular reflection spots reveal the corresponding zone axis along [0 0 1] direction. Regarding the α-Fe_2O_3 sample whose precursor as Fe_3S_4 sample was prepared at 180 °C for 12 h in mixed solvents (EG + H_2O) as 30 mL + 10 mL, the resulting TEM and HRTEM images are shown in Fig. 6e and f. And the information we can learn from them are almost equal to those shown in Fig. 6a–d.

As revealed in Fig. 3, the as-prepared Fe_3S_4 sample can be converted into α-Fe_2O_3 sample at the calcination temperature exceeding 400 °C in air. Furthermore, the weight loss from Fe_3S_4 to α-Fe_2O_3 is 21.62% in theory. To study the oxidation behavior of the Fe_3S_4 sample in detail, which were obtained at 180 °C for 12 h in mixed solvents (EG + H_2O) as 30 mL + 10 mL, we carried out the TGA test by designating the temperature in the range of 25–900 °C, as shown in Fig. 7. We can see that the mass profile has a major weight loss of *ca.* 22% over temperature range of 25–900 °C. This result coincides well with the theoretical value (21.62%) for the conversion of Fe_3S_4 to α-Fe_2O_3 in air. In addition, Fig. 7 tells us that there exists a sharp decline in weight nearby 400 °C, which also agrees well with the XRPD results shown in Fig. 3.

The magnetic properties of the as-obtained Fe_3S_4 samples were recorded by a VSM device. And the typical magnetic hysteresis loops for Fe_3S_4 nanosheets and Fe_3S_4 nanoparticles measured at room temperature are depicted in Fig. 8. The two hysteresis loops almost reach saturation at 10,000 Oe of applied field. In the case of Fe_3S_4 nanosheets shown in Fig. 8a, it reveals a ferromagnetic behavior with the saturation magnetization (M_s) of *ca.* 23.1 emu/g. As for Fe_3S_4 nanoparticles shown in Fig. 8b, it also reveals a ferro-

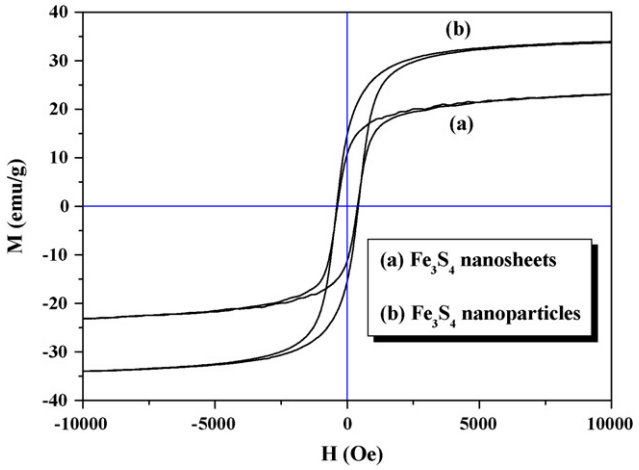

Fig. 8. Room temperature magnetic hysteresis loops for (a) Fe_3S_4 nanosheets, and (b) Fe_3S_4 nanoparticles.

magnetic behavior having the saturation magnetization (M_s) of *ca.* 34.0 emu/g. Clearly, the saturation magnetization of Fe_3S_4 nanoparticles is much higher than that of Fe_3S_4 nanosheets. As well known, magnetic properties are strongly influenced by many parameters, including sizes, shapes, crystallinity, and crystal defects. In general, the saturation magnetization of magnetic particles increase accompanying with the increase in particle size or with the increase in crystallinity [28]. This well accords with the fact that the crystallinity of Fe_3S_4 nanoparticles is much higher than that of Fe_3S_4 nanosheets, as given in Fig. 1a and b. During the magnetic measurement process, the isotropic Fe_3S_4 nanoparticles prefer to align along the magnetic line of force, favoring head-to-tail orientation. It thus results in a relatively higher magnetic saturation value.

4. Conclusion

In summary, a solvothermal synthetic method has been developed to prepare greigite (Fe_3S_4) samples in the mixed solvents of ethylene glycol (EG) and H_2O. By altering the compositon of mixed solvents of EG and H_2O, Fe_3S_4 nanosheets and nanoparticles occurred. Besides, the as-prepared Fe_3S_4 nanomaterials were further converted into hematite (α-Fe_2O_3) by calcination method. It is found that the as-obtained Fe_3S_4 nanosheets and nanoparticles both exhibits a ferromagnetic behaviors. Furthermore, the saturation magnetization of Fe_3S_4 nanoparticles is higher than that of Fe_3S_4 nanosheets owing to their difference in sizes and shapes. The present synthetic method is convenient and repetitious, which might open up an opportunity to prepare other kinds of functional nanomaterials, especially sensitive to the solvent effect.

Acknowledgements

This project was supported by the Scientific Research Foundation for the Returned Overseas Chinese Scholars, Ministry of Education of China and Anhui Provincial Natural Science Foundation (090414194). The authors would gratefully thank Prof. Zheng Hua Wang and Prof. Ming Zai Wu at Anhui Normal University and Anhui University for their kind assistances.

Appendix A. Supplementary data

Supplementary data associated with this article can be found, in the online version, at doi:10.1016/j.jallcom.2009.08.127.

References

[1] Y.W. Jun, J.S. Choi, J.W. Cheon, Angew. Chem. Int. Ed. 45 (2006) 3414.
[2] A.R. Tao, S. Habas, P.D. Yang, Small 4 (2008) 310.
[3] Y.J. Xiong, Y.N. Xia, Adv. Mater. 19 (2007) 3385.
[4] R. Si, Y.W. Zhang, L.P. You, C.H. Yan, Angew. Chem. Int. Ed. 44 (2005) 3256.
[5] L. Manna, A.P. Alivisatos, et al., Nat. Mater. 2 (2003) 382.
[6] S.U. Son, I.K. Park, J. Park, T. Hyeon, Chem. Commun. 7 (2004) 778.
[7] K.H. Park, S.U. Son, et al., Angew. Chem. Int. Ed. 46 (2007) 1152.
[8] B.J. Skinner, R.C. Erd, F.S. Grimaldi, Am. Mineral. 49 (1964) 543.
[9] G.V. Gibbs, D.F. Cox, K.M. Rosso, et al., J. Phys. Chem. B 111 (2007) 1923.
[10] I.F. Snowball, R. Thompson, J. Quat. Sci. 3 (1988) 121.
[11] R.I. Reynolds, J.G. Rosenbaum, et al., J. Paleolimnol. 21 (1999) 193.
[12] I. Letard, Ph. Sainctavit, et al., Phys. Scripta 115 (2005) 489.
[13] J.M.D. Coey, et al., Solid State Commun. 8 (1970) 1605.
[14] M.R. Spender, J.M.D. Coey, A.H. Morrish, Can. J. Phys. 50 (1972) 2313.
[15] X.F. Qian, X.M. Zhang, Y.T. Qian, et al., Mater. Sci. Eng. B 64 (1999) 170.
[16] Z.B. He, S.H. Yu, et al., Adv. Funct. Mater. 16 (2006) 1105.
[17] P.V. Vanitha, P. O'Brien, J. Am. Chem. Soc. 130 (2008) 17256.
[18] X.Y. Chen, Y.T. Qian, et al., Chem. Phys. Lett. 403 (2005) 396.
[19] X.Y. Chen, Z.J. Zhang, et al., Chem. Phys. Lett. 422 (2006) 294.
[20] S.F. Chen, S.H. Yu, et al., Chem. Eur. J. 10 (2004) 3050.
[21] L.S. Zhong, J.S. Hu, L.J. Wan, et al., Adv. Mater. 18 (2006) 2426.
[22] Y.L. Chueh, L.J. Chou, Z.L. Wang, et al., Adv. Funct. Mater. 16 (2006) 2243.
[23] X.G. Wen, Z.L. Wang, S.H. Yang, et al., J. Phys. Chem. B 109 (2005) 215.
[24] X.Y. Chen, Z.J. Zhang, Y.T. Qian, et al., Chem. Phys. Lett. 407 (2005) 482.
[25] Z.J. Zhang, X.Y. Chen, J. Phys. Chem. Solids 70 (2009) 1121.
[26] H.D. Yu, D.S. Wang, M.Y. Han, J. Am. Chem. Soc. 129 (2007) 2333.
[27] H.P. Cong, S.H. Yu, Cryst. Growth Des. 9 (2009) 210.
[28] H.P. Qi, Q.W. Chen, et al., J. Crys. Growth 311 (2009) 394.